A01-25303

42nd AIAA/ASME/ASCE/AHS/ASC Structures, Structural Dynamics, and Materials Conference and Exhibit
Seattle, WA 16-19 April 2001

AIAA-2001-1593

STATISTICAL APPROXIMATIONS FOR CHARACTERISTIC-MODE-BASED POWER FLOW ANALYSIS

Yung-Chang Tan
Matthew P. Castanier
Christophe Pierre *
Vibrations and Acoustics Laboratory
Department of Mechanical Engineering
The University of Michigan
Ann Arbor, Michigan 48109–2125

This paper presents a general statistical treatment for power flow analysis in a complex structure. The nominal power flow is computed using the characteristic constraint (CC) modes of the component structures. These CC modes are built from component mode synthesis (CMS) of finite element models, and they form a highly-reduced order basis for capturing the motion of the interface between components — and thus the power flow. The power flow statistics are then calculated over an ensemble of systems due to the variation of structural system parameters. Each modal response is expanded in a basis of quadrature polynomials or locally linear interpolation (LLI) functions in these uncertain parameters. The system equations for the reduced order CMS model with uncertainties are derived using Galerkin's method. These equations have the same form as the nominal power flow equations, but the number of equations is increased by a factor equal to the order of the polynomials (when using quadrature polynomials) or the number of nodes in the parameter space (when using LLI functions). Thus, the ensemble-averaged power flow can be calculated by solving this new set of equations, instead of using Monte Carlo simulations. A cantilever plate and a L-shaped plate are used as example structures for the demonstration of these statistical approximations. In general, this statistical treatment provides efficient and accurate modeling of parameter uncertainties, which is critical for mid-frequency vibration analysis.

Introduction

In the mid- to high- frequency range, vibration response becomes both expensive to compute and highly sensitive to uncertain physical details of the system. Moreover, many processes that excite noise and vibration are statistical or random in nature. Statistical energy analysis (SEA),[1–3] a widely-used vibration analysis method in the high-frequency range, addresses these challenges by taking a statistical approach to power flow analysis. Power flow is a scalar measurement of the vibration energy transmitted from one part of the structure to the other parts of the structure. It is the core concept for SEA to analyze the energy flow among the component structures. However, SEA becomes less accurate in cases of intermediate or low modal density, which occur in the mid-frequency range. On the other hand, a general statistical treatment based on finite element model (FEM) often employs Monte Carlo simulation techniques to evaluate the statistical moments of the response and power flow. While this approach is versatile and accurate, it incurs prohibitive computational cost. Therefore, the objective of this paper is to present an efficient alternative for statistical power flow analysis by improving upon these methods.

A characteristic-mode-based power flow analysis method has been presented the authors.[4] This paper adds a statistical perspective to the nominal power flow equations shown in Ref. 4. The nominal power flow equations were formulated from a component mode synthesis (CMS)[5,6] approach. In CMS, a component model, such as an FEM, is constructed and analyzed separately for each component structure. The Craig-Bampton method of CMS provides an excellent framework for predicting power flow, since the Craig-Bampton constraint modes capture fully the motion of the interface between component structures. However, since there is necessarily one constraint mode for each FEM degree of freedom of the interface, the cost of this CMS method is still prohibitive for a sufficiently fine mesh. Consequently, a secondary modal analysis reduction technique (SMART) was developed to further reduce the size of the CMS model. For the purpose of predicting power flow, the SMART approach may be applied to the interface between components. In particular, an eigenanalysis is performed on the constraint-mode partitions of the CMS mass and stiffness matrices. The resultant eigenvectors are called characteristic constraint (CC) modes.[7] Reference 4 showed that the power flow is accurately calculated by this reduced-order CMS model with relatively few CC modes.

There are always uncertainties associated with the mathematical modeling of the structural behavior, which result from the numerous idealizations and assumptions made

* Address all correspondence to this author.

when modeling the geometry, the boundary conditions, and the constitutive behavior of the materials involved. Structural systems with uncertainty are usually investigated by stochastic approaches, where the uncertain parameters are described through a joint probability density function (pdf). Monte Carlo simulation is often employed to provide accurate results for the statistical moments that require evaluating multiple integrals over the uncertain parameter space. However, in general, the Monte Carlo method is computationally expensive. An alternative integration technique is Gaussian quadratures or, in multi-dimensional cases, cubatures. Some previous studies[8,9] employed weighted residual methods with those quadrature polynomials to investigate the response variability of general dynamic systems due to the uncertain system parameters. In this paper, this method is employed to compute the ensemble-averaged power flow based on the reduced-order CMS model. In addition, an extension that uses locally linear interpolation functions as a basis to approximate the modal responses is also introduced. These new formulations are seen to accommodate different sources of uncertainties as well as provide much faster convergence of power flow statistics compared to Monte Carlo simulations.

This paper is organized as follows. In the second section, the nominal reduced order model is presented. In the third section, the ensemble-averaged power flow is defined. In the fourth section, the quadrature polynomials are introduced. Then Galerkin's method is applied to the reduced-order CMS model using quadrature polynomials as a basis. Next, the matrix equation for the ensemble-averaged power flow is formulated, and numerical examples are shown. The first example is the cantilever plate system shown in Ref. 4 and 7, in which the variations of component modal stiffnesses are considered. In the second example, the variation of a physical parameter is considered and its effect on power flow is studied for a L-shaped plate. In the fifth section, the ensemble-averaged power flow is formulated using Galerkin's method with locally linear interpolation functions. This approximation is demonstrated numerically by examining the L-shaped plate with three random physical parameters. This work is then summarized in the final section.

Nominal Reduced Order Model

The nominal model (i.e., without uncertainties) is briefly described in this section in order to provide a platform for deriving the statistical approximations. In this paper, the finite element model (FEM) of the full structure is divided into separate component FEMs. The mass and stiffness matrices from each component FEM are first partitioned into the interface submatrices, the interior (omitted DOF) submatrices, and their coupling submatrices. Then, the Craig-Bampton method of component mode synthesis (CMS) is used to generate a reduced order model of the global structure. The Craig-Bampton method utilizes two sets of substructure modes: component normal (N) modes, $\mathbf{\Phi}_i^N$, and constraint (C) modes, $\mathbf{\Phi}_i^C$, where i denotes the i-th component structure. The component FEM matrices are transformed by $\mathbf{\Phi}_i^N$ and $\mathbf{\Phi}_i^C$ such that only the component modal DOF and the interface DOF are retained. The retained DOF are then used to couple respectively the mass and stiffness matrices of the connected component structures into those of the entire structure. This synthesis yields the modal velocity vector, $\mathbf{v}^{CMS}$, of the synthesized system to be partitioned as

$$\mathbf{v}^{CMS} = \begin{bmatrix} \mathbf{v}^{C^T} & \mathbf{v}_1^{N^T} & \mathbf{v}_2^{N^T} & \cdots & \mathbf{v}_{n^{ss}}^{N^T} \end{bmatrix}^T \tag{1}$$

where n^{ss} is the number of substructures contained in the global structure. The corresponding synthesized CMS mass and stiffness matrices have the following forms

$$\mathbf{M}^{CMS} = \begin{bmatrix} \bar{\mathbf{m}}^C & \mathbf{m}_1^{CN} & \mathbf{m}_2^{CN} & \cdots & \mathbf{m}_{n^{ss}}^{CN} \\ \mathbf{m}_1^{CN^T} & \mathbf{m}_1^N & \mathbf{0} & \cdots & \mathbf{0} \\ \mathbf{m}_2^{CN^T} & \mathbf{0} & \mathbf{m}_2^N & & \mathbf{0} \\ \vdots & \vdots & & \ddots & \vdots \\ \mathbf{m}_{n^{ss}}^{CN^T} & \mathbf{0} & \mathbf{0} & \cdots & \mathbf{m}_{n^{ss}}^N \end{bmatrix} \tag{2}$$

$$\mathbf{K}^{CMS} = \begin{bmatrix} \bar{\mathbf{k}}^C & \mathbf{0} & \mathbf{0} & \cdots & \mathbf{0} \\ \mathbf{0} & \mathbf{k}_1^N & \mathbf{0} & \cdots & \mathbf{0} \\ \mathbf{0} & \mathbf{0} & \mathbf{k}_2^N & & \mathbf{0} \\ \vdots & \vdots & & \ddots & \vdots \\ \mathbf{0} & \mathbf{0} & \mathbf{0} & \cdots & \mathbf{k}_{n^{ss}}^N \end{bmatrix} \tag{3}$$

where component modal matrices $\mathbf{m}_i^N$ and $\mathbf{k}_i^N$, for $i = 1, 2, \ldots, n^{ss}$, are diagonalized and their sizes depend on the number of modes one selects for the frequency range of interest. However, the number of constraint-mode DOF, or the size of matrices, $\bar{\mathbf{m}}^C$ and $\bar{\mathbf{k}}^C$, is equal to the number of DOF in the interface of the FEM, so it is determined by the finite element mesh. If the mesh is fine in the interface region, then the constraint-mode partitions of the CMS matrices may be relatively large. Hence, the authors[7] proposed a technique to further reduce the CMS matrices by performing a modal analysis on the constraint-mode DOF

$$\bar{\mathbf{k}}^C \boldsymbol{\psi}_n = \Lambda_n \bar{\mathbf{m}}^C \boldsymbol{\psi}_n \quad \text{for } n = 1, 2, 3, \ldots \tag{4}$$

These eigenvectors, $\boldsymbol{\psi}_n$, may be transformed into the finite element DOF for component structure i using the following transformation

$$\mathbf{\Phi}_i^{CC} = \mathbf{\Phi}_i^C \boldsymbol{\beta}_i^C \mathbf{\Psi} \tag{5}$$

where $\mathbf{\Psi} = [\boldsymbol{\psi}_1 \ \boldsymbol{\psi}_2 \ \cdots \ \boldsymbol{\psi}_{n^{cc}}]$ is a selected set of the interface eigenvectors with n^{cc} indicating the number of the selected eigenvectors. n^{cc} is relatively small compared to the number of the constraint-mode DOF. $\boldsymbol{\beta}_i^C$ is the matrix that maps the global (system) interface DOF, $\mathbf{v}^C$, back to the local (subsystem i) DOF, $\mathbf{v}_i^C$. Furthermore, $\mathbf{\Phi}_i^{CC}$ are referred to as the characteristic constraint (CC) modes, because they represent the characteristic physical motion associated with the constraint modes. The benefit of using CC modes is shown in the efficient computation of the power flow through the interface between the connected

component structures. Relatively few CC-mode DOF are employed in this calculation compared to the number of interface-node DOF in the FEM.

Finally, the CMS matrices can be transformed by CC modes such that the reduced order CMS matrices can be obtained with the same form[4] as Eqs. (2) and (3) and the unknown velocity vector $\mathbf{v}^{ROM}$ now is partitioned as

$$\mathbf{v}^{ROM} = \left[\begin{array}{ccccc} \mathbf{v}^{CC^T} & \mathbf{v}_1^{N^T} & \mathbf{v}_2^{N^T} & \cdots & \mathbf{v}_{n^{ss}}^{N^T} \end{array} \right]^T \quad (6)$$

where superscript CC indicates that the partition is associated with the CC modes. The equations of motion of the reduced order CMS model (ROM) can be expressed by

$$\frac{1}{j\omega}\left[-\omega^2 \mathbf{M}^{ROM} + (1+j\eta)\,\mathbf{K}^{ROM}\right]\mathbf{v}^{ROM} = \mathbf{f}^{ROM} \quad (7)$$

The mass matrix, $\mathbf{M}^{ROM}$, the stiffness matrix, $\mathbf{K}^{ROM}$, and the applied force vector, $\mathbf{f}^{ROM}$, can be explicitly written as

$$\mathbf{M}^{ROM} = \left[\begin{array}{ccccc} \bar{\mathbf{m}}^{CC} & \bar{\mathbf{m}}_1^{CN} & \bar{\mathbf{m}}_2^{CN} & \cdots & \bar{\mathbf{m}}_{n^{ss}}^{CN} \\ \bar{\mathbf{m}}_1^{CN^T} & \mathbf{m}_1^N & \mathbf{0} & \cdots & \mathbf{0} \\ \bar{\mathbf{m}}_2^{CN^T} & \mathbf{0} & \mathbf{m}_2^N & & \mathbf{0} \\ \vdots & \vdots & & \ddots & \vdots \\ \bar{\mathbf{m}}_{n^{ss}}^{CN^T} & \mathbf{0} & \mathbf{0} & \cdots & \mathbf{m}_{n^{ss}}^N \end{array} \right] \quad (8)$$

$$\mathbf{K}^{ROM} = \left[\begin{array}{ccccc} \bar{\mathbf{k}}^{CC} & \mathbf{0} & \mathbf{0} & \cdots & \mathbf{0} \\ \mathbf{0} & \mathbf{k}_1^N & \mathbf{0} & \cdots & \mathbf{0} \\ \mathbf{0} & \mathbf{0} & \mathbf{k}_2^N & & \mathbf{0} \\ \vdots & \vdots & & \ddots & \vdots \\ \mathbf{0} & \mathbf{0} & \mathbf{0} & \cdots & \mathbf{k}_{n^{ss}}^N \end{array} \right] \quad (9)$$

$$\mathbf{f}^{ROM} = \left[\begin{array}{ccccc} \mathbf{f}^{CC^T} & \mathbf{f}_1^{N^T} & \mathbf{f}_2^{N^T} & \cdots & \mathbf{f}_{n^{ss}}^{N^T} \end{array} \right]^T \quad (10)$$

where

$$\bar{\mathbf{m}}^{CC} = \boldsymbol{\Psi}^T \bar{\mathbf{m}}^C \boldsymbol{\Psi}, \quad \bar{\mathbf{k}}^{CC} = \boldsymbol{\Psi}^T \bar{\mathbf{k}}^C \boldsymbol{\Psi} \quad (11)$$

and

$$\bar{\mathbf{m}}_i^{CN} = \boldsymbol{\Psi}^T \, \boldsymbol{\beta}_i^{C^T} \mathbf{m}_i^{CN} \quad (12)$$

The partitions of the ROM matrices can be used to formulate the power flow. The power flowing out of component structure i at a discrete frequency ω through the interface with other directly connected component structures can be defined by

$$\Pi_i(\omega) = -\frac{1}{2\pi}\lim_{T\to 0}\frac{1}{2T} E_t\left[\mathrm{Re}\left\{\mathbf{t}_i\,(\omega;T)^*\,\mathbf{v}_i^C\,(\omega;T)\right\}\right] \quad (13)$$

where $E_t[\,]$ denotes the expected value with respect to time, $\mathbf{t}_i$ is the traction force vector, and $\mathbf{v}_i^C$ is the corresponding velocity vector on the interface. The power flow results are formulated with respect to the CC-mode degrees of freedom (DOF) instead of the much larger set of interface DOF. The detailed derivations were presented by the authors in Ref. 4. An alternative formulation that may yield efficient computation is achieved by projecting the power flow onto the global modes of the ROM. First, an eigenanalysis is performed

$$\mathbf{K}^{ROM}\boldsymbol{\Gamma} = \mathbf{M}^{ROM}\boldsymbol{\Gamma}\boldsymbol{\Lambda} \quad (14)$$

where the eigenmatrix $\boldsymbol{\Gamma}$ can be partitioned as

$$\boldsymbol{\Gamma} = \left[\begin{array}{ccccc} \boldsymbol{\gamma}^{CC^T} & \boldsymbol{\gamma}_1^{N^T} & \boldsymbol{\gamma}_2^{N^T} & \cdots & \boldsymbol{\gamma}_{n^{ss}}^{N^T} \end{array} \right]^T \quad (15)$$

The mass and stiffness matrices can be diagonalized by using $\boldsymbol{\Gamma}$. As a result, Eq. (7) can be transformed to

$$\frac{1}{j\omega}\left[-\omega^2 \bar{\mathbf{M}} + (1+j\eta)\,\bar{\mathbf{K}}\right]\bar{\mathbf{v}} = \bar{\mathbf{f}} \quad (16)$$

where

$$\bar{\mathbf{M}} = \boldsymbol{\Gamma}^T \mathbf{M}^{ROM}\boldsymbol{\Gamma}, \quad \bar{\mathbf{K}} = \boldsymbol{\Gamma}^T \mathbf{K}^{ROM}\boldsymbol{\Gamma}, \quad \bar{\mathbf{f}} = \boldsymbol{\Gamma}^T \mathbf{f}^{ROM} \quad (17)$$

Considering time-harmonic excitation, the power flow can be formulated in terms of $\bar{\mathbf{v}}$

$$\Pi_i(\omega) = \frac{1}{2}\,\mathrm{Re}\left[\bar{\mathbf{f}}_i^*\bar{\mathbf{v}}\right] - \frac{1}{2}\bar{\mathbf{v}}^*\bar{\mathbf{C}}_i\bar{\mathbf{v}} \quad (18)$$

where $\bar{\mathbf{C}}_i$ is the damping of substructure i projected onto the global modes of the ROM

$$\bar{\mathbf{C}}_i = \boldsymbol{\gamma}^{CC^T}\,\mathrm{Re}\left[\mathbf{z}_i^{CC}\right]\boldsymbol{\gamma}^{CC} + \boldsymbol{\gamma}_i^{N^T}\,\mathrm{Re}\left[\mathbf{z}_i^{N}\right]\boldsymbol{\gamma}_i^{N} \quad (19)$$

where $\mathbf{z}_i^{CC}$ is the impedance matrix of substructure i associated with CC modes, and $\mathbf{z}_i^N$ the impedance matrix of substructure i associated with component modes. Furthermore, $\bar{\mathbf{f}}_i$ is given by

$$\bar{\mathbf{f}}_i = \boldsymbol{\gamma}_i^{N^T}\mathbf{f}_i^N + \boldsymbol{\gamma}^{CC^T}\mathbf{f}_i^{CC} \quad (20)$$

where $\mathbf{f}_i^{CC}$ is the applied force on substructure i associated with CC modes.

Approximations of Ensemble-Averaged Power Flow

The uncertainties associated with the system require non-deterministic modeling of the system parameters in order to predict the statistics of the forced response. It is assumed that the system is represented by an ensemble — a population of similar systems with statistically-described variations in properties. A set of uncorrelated random variables are used to quantify the uncertainties associated with the discrete parameters of the ROM. Therefore, the ensemble-averaged power flow spectral density, $E_{\boldsymbol{\theta}}\left[\Pi_i(\omega;\boldsymbol{\theta})\right]$, relative to this uncorrelated set of random variables, θ_s, for $s = 1, 2, ..., n^{\theta}$, is given by

$$E_{\boldsymbol{\theta}}\left[\Pi_i(\omega;\boldsymbol{\theta})\right] = -\frac{1}{2\pi}\lim_{T\to 0}\frac{1}{2T} E_t\left[\mathrm{Re}\left\{E_{\boldsymbol{\theta}}\left[\,\mathbf{t}_i\,(\omega;\boldsymbol{\theta};T)^*\,\mathbf{v}_i^C\,(\omega;\boldsymbol{\theta};T)\right]\right\}\right] \quad (21)$$

where $\boldsymbol{\theta} = [\ \theta_1 \quad \theta_2 \quad \ldots \quad \theta_{n^\theta}\ ]^T$ and the operator $E_{\boldsymbol{\theta}}[\ \cdot\ ]$ indicates

$$E_{\boldsymbol{\theta}}[\ \cdot\ ] = \int_{\theta_{n^\theta}} \cdots \int_{\theta_2} \int_{\theta_1} [\ \cdot\ ] \prod_{s=1}^{n^\theta} p(\theta_s)\ d\theta_1 d\theta_2 \cdots d\theta_{n^\theta}$$

where $p(\theta_s)$ is the probability density function (pdf) of θ_s. The challenge in evaluating the ensemble average thus becomes performing multiple integrals over the parameter space. Furthermore, $E_{\boldsymbol{\theta}}\left[\mathbf{t}_i^* \mathbf{v}_i^C\right]$ in Eq. (21) can be expanded in terms of CC-mode velocity vector $\mathbf{v}^{CC}$, for $i = 1, 2, ..., n^{ss}$, as

$$\begin{aligned} E_{\boldsymbol{\theta}}\left[\mathbf{t}_i^* \mathbf{v}_i^C\right] &= E_{\boldsymbol{\theta}}\left[\mathbf{v}^{CC^*} \mathbf{z}_i^{CC^*} \mathbf{v}^{CC}\right] \\ &\quad - j\omega E_{\boldsymbol{\theta}}\left[\mathbf{v}_i^{N^*} \bar{\mathbf{m}}_i^{CN^T} \mathbf{v}^{CC}\right] \\ &\quad - E_{\boldsymbol{\theta}}\left[\mathbf{f}_i^{CC^*} \mathbf{v}^{CC}\right] \end{aligned} \tag{22}$$

A general numerical integration scheme other than Monte Carlo methods is needed for the evaluation of the three terms on the right-hand-side of Eq. (22).

Galerkin's Method with Quadrature Polynomials

Gaussian Quadratures

The Gaussian quadrature method is a commonly used numerical technique to approximate an integral. The treatment of Gaussian quadratures consists in finding a set of polynomials, $P_i(\theta_s)$, for $i = 1, 2, \ldots$, satisfying the orthogonality relationship over a weight function $W(\theta_s)$

$$\int_{\theta_s} W(\theta_s) P_i(\theta_s) P_j(\theta_s)\, d\theta_s = \delta_{ij} \tag{23}$$

where P_i and P_j are polynomials of order i and j, respectively. If the weight function is given by

$$W(\theta_s) = 1 \text{ for } -1 < \theta_s < 1 \tag{24}$$

the normalized Legendre polynomials will satisfy Eq. (23), and they are defined as

$$P_0 = \sqrt{\frac{1}{2}},\ P_1(\theta_s) = \sqrt{\frac{3}{2}}\theta_s,\ P_2(\theta_s) = \sqrt{\frac{5}{2}}\frac{3\theta_s^2 - 1}{2}, \ldots$$

This set of polynomials also satisfy the following recurrence relation

$$\theta_s P_i(\theta_s) = L_i P_{i-1}(\theta_s) + L_{i+1} P_{i+1}(\theta_s) \tag{25}$$

where

$$L_i = \frac{i}{\sqrt{(2i-1)(2i+1)}} \tag{26}$$

This choice of weight function is equivalent to assigning to each random variable θ_s a uniformly distributed pdf over the range $[-1, 1]$. Some other classical, well-studied, orthogonal polynomials are associated with different pdfs to enable fast convergence of the integration. For example, Hermite polynomials are suited for a normally distributed pdf.[9]

Galerkin's Method

The quadrature rules suggest that, for a given pdf, one can find a corresponding set of orthogonal polynomials as a basis to approximate the unknowns — modal velocities — in the ROM matrix equations. By applying Galerkin's method, the integral will be reduced to an algebraic matrix equation, and then the modal velocities can be solved in terms of the random parameters at each discrete frequency. As a result, the statistical moments of power flow can be evaluated using these modal velocities.

The equation of motion of the ROM, Eq. (7), with the random parameters $\boldsymbol{\theta}$ can be cast in the form

$$\sum_{b=1}^{n^{ROM}} z_{ab}(\omega;\boldsymbol{\theta}) v_b(\omega;\boldsymbol{\theta}) = f_a(\omega) \quad \text{for } a = 1, 2, ..., n^{ROM} \tag{27}$$

where $v_b(\omega;\boldsymbol{\theta})$ is the b-th component of the velocity vector $\mathbf{v}^{ROM}$; $f_a(\omega)$ is the a-th component of the applied force vector $\mathbf{f}^{ROM}$; and $z_{ab}(\omega;\boldsymbol{\theta})$ is an impedance component of the ROM, which can be explicitly expressed by

$$z_{ab}(\omega;\boldsymbol{\theta}) = \frac{1}{j\omega}\left[-\omega^2 m_{ab}(\boldsymbol{\theta}) + (1 + j\eta) k_{ab}(\boldsymbol{\theta})\right] \tag{28}$$

where m_{ab} is an element of the mass matrix $\mathbf{M}^{ROM}$ and k_{ab} is an element of the stiffness matrix $\mathbf{K}^{ROM}$. Equation (27) is general and does not show the special form of the ROM, where some of the impedance components are null. This general formulation is intended to accommodate different sources of uncertainty from a variety of cases. In addition, quadratic polynomial approximation is used to represent the impedance components

$$\begin{aligned} z_{ab}(\omega;\boldsymbol{\theta}) &= z_{0ab}(\omega) + \sum_{r=1}^{n^\theta} z_{1abr}(\omega)\theta_r \\ &\quad + \sum_{r=1}^{n^\theta}\sum_{s=1}^{n^\theta} z_{2abrs}(\omega)\theta_r\theta_s \end{aligned} \tag{29}$$

Polynomials of higher degree or cubic splines may be desirable to approximate more dramatic variations. Generally, it should be noted that the approximation in terms of $\boldsymbol{\theta}$ cannot be derived analytically from an arbitrary FEM. The coefficients in Eq. (29) are usually obtained numerically by least-square fit. This process is itself computationally intensive. Consequently, it would be a trade-off to obtain an approximation with only low degrees of polynomials if the system varies smoothly due to the uncertainty. Considering a uniformly distributed pdf, each modal velocity $v_b(\omega;\boldsymbol{\theta})$ is approximated by Legendre polynomials as

$$v_b(\omega;\boldsymbol{\theta}) = \sum_{0 \le |\mathbf{l}| \le n^p} w_{bl_1 l_2 \cdots l_{n^\theta}}(\omega) \prod_{s=1}^{n^\theta} P_{l_s}(\theta_s)$$
$$\text{for } b = 1, 2, ..., n^{ROM} \tag{30}$$

where

$$|\mathbf{l}| = l_1 + l_2 + \cdots + l_{n^\theta} \tag{31}$$

n^p is the order of approximation in the random space of variables $\boldsymbol{\theta}$. It can be shown that the number of unknown coefficients, $w_{bl_1l_2\cdots l_{n^\theta}}(\omega)$, in the approximation is[8]

$$n^d = \frac{(n^p + n^\theta)!}{n^p! n^\theta!} \tag{32}$$

After substituting Eq. (30) for v_b and Eq. (29) for z_{ab} in Eq. (27), one can apply Galerkin's method due to the orthogonality of Legendre polynomials. With the help of Eqs. (23) and (25), Eq. (27) can be reduced to

$$\begin{aligned}
&\sum_{b=1}^{n^{ROM}} \Bigg\{ z_{0ab} w_{bl_1l_2\cdots l_{n^\theta}} + \sum_{r=1}^{n^\theta} z_{1abr} \\
&\left(L_{l_r} w_{bl_1\cdots l_r-1\cdots l_{n^\theta}} + L_{l_r+1} w_{bl_1\cdots l_r+1\cdots l_{n^\theta}}\right) \\
&+ \sum_{r=1}^{n^\theta} \sum_{\substack{s=1 \\ s\neq r}}^{n^\theta} z_{2abrs} \left(L_{l_r} L_{l_s} w_{bl_1\cdots l_r-1\cdots l_s-1\cdots l_{n^\theta}}\right. \\
&+ L_{l_r} L_{l_s+1} w_{bl_1\cdots l_r-1\cdots l_s+1\cdots l_{n^\theta}} \\
&+ L_{l_r+1} L_{l_s} w_{bl_1\cdots l_r+1\cdots l_s-1\cdots l_{n^\theta}} \\
&\left. + L_{l_r+1} L_{l_s+1} w_{bl_1\cdots l_r+1\cdots l_s+1\cdots l_{n^\theta}}\right) \\
&+ \sum_{r=1}^{n^\theta} z_{2abrr} \left(L_{l_r} L_{l_r-1} w_{bl_1\cdots l_r-2\cdots l_{n^\theta}}\right. \\
&+ \left(L_{l_r}^2 + L_{l_r+1}^2\right) w_{bl_1\cdots l_r\cdots l_{n^\theta}} \\
&\left. + L_{l_r+1} L_{l_r+2} w_{bl_1\cdots l_r+2\cdots l_{n^\theta}}\right)\Bigg\} \\
= \; & 2^{n^\theta/2} f_a \prod_{s=1}^{n^\theta} \delta_{l_s 0} \quad \text{for } a = 1, 2, ..., n^{ROM}
\end{aligned} \tag{33}$$

where L_l are the coefficients given by Eq. (26). The unknowns $w_{bl_1l_2\cdots l_{n^\theta}}$ can be rearranged into an $n^{ROM} \times n^d$ dimensional column vector $\mathbf{w}$, which can be described by its CC-mode and component partitions as

$$\mathbf{w} = \begin{bmatrix} \mathbf{w}^{CC^T} & \mathbf{w}_1^{N^T} & \mathbf{w}_2^{N^T} & \cdots & \mathbf{w}_{n^{ss}}^{N^T} \end{bmatrix}^T \tag{34}$$

Eq. (33) can be put in a matrix form as

$$\hat{\mathbf{Z}}\mathbf{w} = \hat{\mathbf{f}} \tag{35}$$

The components of the matrix $\hat{\mathbf{Z}}$ correspond to all the impedance coefficients on the left-hand-side of Eq. (33) and can be partitioned as

$$\hat{\mathbf{Z}} = \begin{bmatrix} \hat{\mathbf{z}}^{CC}(\omega) & j\omega\hat{\mathbf{m}}_1^{CN} & j\omega\hat{\mathbf{m}}_2^{CN} & \cdots & j\omega\hat{\mathbf{m}}_{n^{ss}}^{CN} \\ j\omega\hat{\mathbf{m}}_1^{CN^T} & \hat{\mathbf{z}}_1^N(\omega) & \mathbf{0} & \cdots & \mathbf{0} \\ j\omega\hat{\mathbf{m}}_2^{CN^T} & \mathbf{0} & \hat{\mathbf{z}}_2^N(\omega) & & \mathbf{0} \\ \vdots & \vdots & & \ddots & \vdots \\ j\omega\hat{\mathbf{m}}_{n^{ss}}^{CN^T} & \mathbf{0} & \mathbf{0} & \cdots & \hat{\mathbf{z}}_{n^{ss}}^N(\omega) \end{bmatrix} \tag{36}$$

where $\hat{\mathbf{z}}^{CC}(\omega) = \sum_{i=1}^{n^{ss}} \hat{\mathbf{z}}_i^{CC}(\omega)$ is sum of the CC-mode partitions of the component impedances. The components of the column vector $\hat{\mathbf{f}}$ correspond to the modal forces on the right-hand-side of Eq. (33) and can be written as

$$\hat{\mathbf{f}} = \begin{bmatrix} \hat{\mathbf{f}}^{CC^T} & \hat{\mathbf{f}}_1^{N^T} & \hat{\mathbf{f}}_2^{N^T} & \cdots & \hat{\mathbf{f}}_{n^{ss}}^{N^T} \end{bmatrix}^T \tag{37}$$

where $\hat{\mathbf{f}}^{CC} = \sum_{i=1}^{n^{ss}} \hat{\mathbf{f}}_i^{CC}$ is sum of the CC-mode partitions of the external component forces. Using the partitions shown in Eq. (36) and Eq. (37), one is now able to approximate the right-hand-side of Eq. (22) as follows

$$\begin{aligned}
&E_{\boldsymbol{\theta}}\left[\mathbf{v}^{CC^*}(\omega;\boldsymbol{\theta})\, \mathbf{z}_i^{CC^*}(\omega;\boldsymbol{\theta})\, \mathbf{v}^{CC}(\omega;\boldsymbol{\theta})\right] \\
= \; & 2^{-n^\theta} \mathbf{w}^{CC^*}(\omega)\, \hat{\mathbf{z}}_i^{CC^*}(\omega)\, \mathbf{w}^{CC}(\omega)
\end{aligned} \tag{38}$$

$$\begin{aligned}
&-j\omega E_{\boldsymbol{\theta}}\left[\mathbf{v}_i^{N^*}(\omega;\boldsymbol{\theta})\, \bar{\mathbf{m}}_i^{CN^*}(\boldsymbol{\theta})\, \mathbf{v}^{CC}(\omega;\boldsymbol{\theta})\right] \\
= \; & -2^{-n^\theta} j\omega \mathbf{w}_i^{N^*}(\omega)\, \hat{\mathbf{m}}_i^{CN^T} \mathbf{w}^{CC}(\omega)
\end{aligned} \tag{39}$$

$$\begin{aligned}
&-E_{\boldsymbol{\theta}}\left[\mathbf{f}_i^{CC^*}(\omega)\, \mathbf{v}^{CC}(\omega;\boldsymbol{\theta})\right] \\
= \; & -2^{-n^\theta/2} \hat{\mathbf{f}}_i^{CC^*}(\omega)\, \mathbf{w}^{CC}(\omega)
\end{aligned} \tag{40}$$

Furthermore, solving for the unknowns, $\mathbf{w}$, from Eq. (35) and substituting them into Eqs. (38), (39), and (40), one can obtain the ensemble-averaged power flow as

$$E_{\boldsymbol{\theta}}\left[\Pi_i(\omega;\boldsymbol{\theta})\right] = \mathrm{tr}\left\{\mathrm{Re}\left[\hat{\mathbf{S}}_i\hat{\mathbf{Y}}\right]\right\} - \mathrm{tr}\left\{\hat{\mathbf{S}}\hat{\mathbf{Y}}^*\hat{\mathbf{C}}_i\hat{\mathbf{Y}}\right\} \tag{41}$$

where

$$\hat{\mathbf{C}}_i = \mathrm{Re}\left[\hat{\mathbf{z}}_i^{CC} + \omega^2 \hat{\mathbf{m}}_i^{CN}\, \hat{\mathbf{z}}_i^{N\,-1}\, \hat{\mathbf{m}}_i^{CN^T}\right] \tag{42}$$

$$\hat{\mathbf{Y}} = \left[\sum_{i=1}^{n^{ss}} \left(\hat{\mathbf{z}}_i^{CC} + \omega^2 \hat{\mathbf{m}}_i^{CN}\, \hat{\mathbf{z}}_i^{N\,-1}\, \hat{\mathbf{m}}_i^{CN^T}\right)\right]^{-1} \tag{43}$$

$$\begin{aligned}
\hat{\mathbf{S}}_i = \; & -\frac{1}{2\pi} \lim_{T\to 0} \frac{1}{2T} E_t \left[\hat{\mathbf{f}}^{CC} \hat{\mathbf{f}}_i^{CC^*} + j\omega \hat{\mathbf{f}}^{CC} \hat{\mathbf{f}}_i^{N^*}\right. \\
& \left. - j\omega \sum_{a=1}^{n^{ss}} \hat{\mathbf{f}}_a^N \hat{\mathbf{f}}_i^{CC^*} + \omega^2 \sum_{a=1}^{n^{ss}} \hat{\mathbf{f}}_a^N \hat{\mathbf{f}}_i^{N^*}\right]
\end{aligned} \tag{44}$$

$$\hat{\mathbf{S}} = \sum_{i=1}^{n^{ss}} \hat{\mathbf{S}}_i \tag{45}$$

Variation of Modal Parameters

The cantilever rectangular plate shown in Fig. 1 is now used as an example structure. For the purpose of this study, this structure is considered to be made of two directly connected substructures — Plate 1 and Plate 2. The FEM and the CMS models were built and the frequencies were carefully examined in Ref. 7. In addition, the deterministic frequency response of power flow in this structure has been investigated in Ref. 4.

Now suppose that each substructure is subjected to modeling errors of material properties. In addition, component

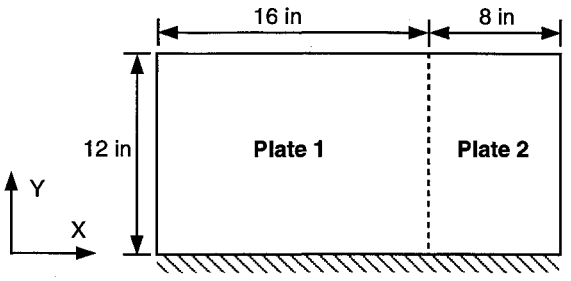

Fig. 1 A cantilever rectangular plate partitioned into two substructures. The dimensions and material properties are the same as those used in Ref.:[10] 2024-T3 aluminum, Young's modulus $E = 10.5 \times 10^6$ psi, Poisson's ratio $\nu = 0.33$, density $\rho = 0.101$ lb/in^3, thickness $t = 0.125$ in.

modes in the mid- to high-frequency range may be more sensitive to these modeling errors. Consequently, the component modal stiffnesses of each substructure are assumed to have uncertain variations from the nominal case. These uncertainties are incorporated into the model by assuming that each component mode group is associated with a random variable with uniform distribution. Thus the impedances in Eq. (27) are

$$z_{ab}(\omega;\theta_1,\theta_2) = j\omega m_{ab} + \frac{\eta - j}{\omega} k_{ab} + \frac{\eta - j}{\omega} k_{ab} \sum_{i=1}^{2} \varepsilon_{iab}\theta_i \tag{46}$$

where m_{ab} and k_{ab} are the mass and stiffness coefficients, η is the damping coefficient and ε_{iab} is given by

$$\varepsilon_{iab} = \begin{cases} \epsilon, \text{ if } n^{cc} + 1 + \sum_{j=1}^{i-1} n_j \le a = b \\ \qquad\qquad \le n^{cc} + \sum_{j=1}^{i} n_j \\ 0, \text{ otherwise} \end{cases} \tag{47}$$

where n^{cc} is the number of retained CC modes and n_j is the number of retained component modes for the jth substructure. Two cases of variation strength are considered so that ϵ is chosen to be $0.05\sqrt{3}$ and $0.10\sqrt{3}$, which correspond to standard deviations equal to 5% and 10% of their nominal values. For both cases, the ensemble-averaged power flow from Plate 1 to Plate 2 is calculated while Plate 1 is subjected to rain-on-the-roof excitation (the excitation that is spatially uncorrelated). The numerical calculation is carried out by using Monte Carlo simulations and two other approximations using Eq. (41) with polynomials of order 3 and order 5 ($n^p = 3$ and 5 in Eq. (30)). The Monte Carlo results are calculated from the power flow equation[4] with 10,000 realizations, which is more than the number needed for the convergence of the solution. Thus the Monte Carlo results are used here as a benchmark for comparing other approximations.

Figure 2 shows that for $\epsilon = 0.05\sqrt{3}$, the results using polynomials of order 3 are in good agreement with the Monte Carlo results. However, in the case $\epsilon = 0.10\sqrt{3}$, as shown in Fig. 3, this approximation could not provide accurate results for this larger range of uncertainties. On the other hand, the Monte Carlo results in Fig. 3 are well approximated by using polynomials of order 5. Since using higher-order polynomials results in finer resolution over the random parameter space, more dramatic changes in the modal response can be captured using the approximations with higher- order polynomials.

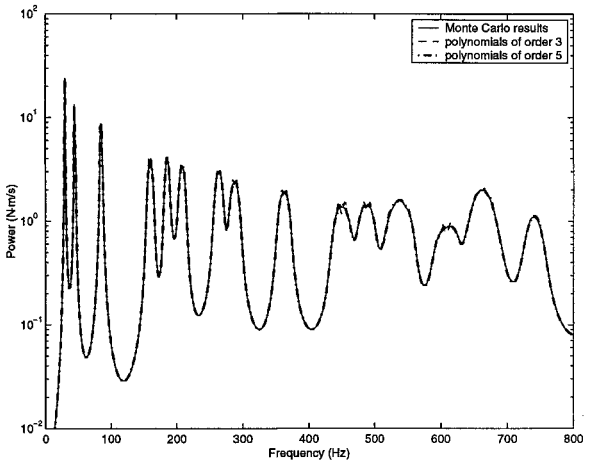

Fig. 2 The ensemble-averaged power flow from Plate 1 to Plate 2 calculated by Monte Carlo methods and the polynomial approximations. The standard deviations of component modal stiffnesses are equal to 5% of their nominal values.

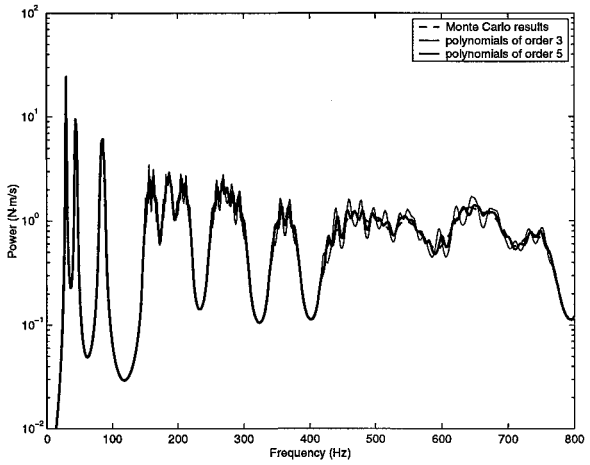

Fig. 3 The ensemble-averaged power flow from Plate 1 to Plate 2 calculated by Monte Carlo methods and the polynomial approximations. The standard deviations of component modal stiffnesses are equal to 10% of their nominal values.

Variation of Physical Parameters

The calculation of $\hat{\mathbf{Y}}$ in Eq. (43) induces considerable amount of computation effort since it requires inverting a full matrix. Thus, the statistical approximation is now applied to an alternative power flow formulation that uses a basis of global modes of the ROM. Even after the expansion resulting from Galerkin's method, all the coupling elements in the system impedance matrix are still very close to the diagonal, resulting in a banded matrix. As a result, this new formulation yields more reduction of computation cost.

If the platform is now chosen to be Eq. (16) instead of

Eq. (7), then Eq. (27) can be reduced to

$$\bar{z}_s(\omega;\boldsymbol{\theta})\,\bar{v}_s(\omega;\boldsymbol{\theta}) = \bar{f}_s(\omega;\boldsymbol{\theta}) \quad \text{for } s = 1,...,n^{ROM} \tag{48}$$

where $\bar{z}_s$, for $s = 1,2,...,n^{ROM}$, are the diagonal elements of the impedance matrix $\bar{\mathbf{Z}}$

$$\bar{\mathbf{Z}} = \frac{1}{j\omega}\left[-\omega^2\bar{\mathbf{M}} + (1+j\eta)\,\bar{\mathbf{K}}\right] \tag{49}$$

where $\bar{\mathbf{K}}$ and $\bar{\mathbf{M}}$ are given by Eq. (17). When the uncertain parameters $\boldsymbol{\theta}$ are incorporated into this platform, $\bar{v}_s$ is approximated by polynomials in terms of $\boldsymbol{\theta}$ with unknown coefficients that can be re-ordered to be $\bar{\mathbf{w}}_s$. By applying Galerkin's method with Legendre polynomials to Eq. (48), an equation similar to Eq. (33) may be derived and put into matrix form:

$$\hat{\mathbf{z}}_s\bar{\mathbf{w}}_s = \mathbf{f}_s \quad \text{for } s = 1,2,...,n^{ROM} \tag{50}$$

Then the unknown vectors, $\bar{\mathbf{w}}_s$, can be solved from Eq. (50). Next, Eq. (18) can be expressed as

$$\Pi_i(\omega;\boldsymbol{\theta}) = \frac{1}{2}\sum_{s=1}^{n^{ROM}} \mathrm{Re}\left[\bar{f}_{is}(\omega;\boldsymbol{\theta})^*\,\bar{v}_s(\omega;\boldsymbol{\theta})\right] - \frac{1}{2}\sum_{r=1}^{n^{ROM}}\sum_{s=1}^{n^{ROM}} \bar{v}_r(\omega;\boldsymbol{\theta})^*\,\bar{C}_{irs}(\omega;\boldsymbol{\theta})\bar{v}_s(\omega;\boldsymbol{\theta}) \tag{51}$$

where $\bar{f}_{is}$, $\bar{C}_{irs}$, and $\bar{v}_s$ are components of matrices $\bar{\mathbf{f}}_i$, $\bar{\mathbf{C}}_i$, and vector $\bar{\mathbf{v}}$, respectively. Furthermore, the ensemble-averaged power flow is represented by

$$\begin{aligned} &E_{\boldsymbol{\theta}}\left[\Pi_i(\omega;\boldsymbol{\theta})\right] \\ &= \frac{1}{2}\sum_{s=1}^{n^{ROM}} \mathrm{Re}\left[\int_\Omega p(\boldsymbol{\theta})\,\bar{f}_{is}(\omega;\boldsymbol{\theta})^*\,\bar{v}_s(\omega;\boldsymbol{\theta})d\Omega\right] \\ &\quad -\frac{1}{2}\sum_{r=1}^{n^{ROM}}\sum_{s=1}^{n^{ROM}}\int_\Omega p(\boldsymbol{\theta})\,\bar{v}_r(\omega;\boldsymbol{\theta})^* \\ &\quad \bar{C}_{rs}(\omega;\boldsymbol{\theta})\bar{v}_s(\omega;\boldsymbol{\theta})d\Omega \end{aligned} \tag{52}$$

where Ω denotes the domain of $\boldsymbol{\theta}$. Next, the following assumptions are considered: $\bar{f}_{is}(\omega;\boldsymbol{\theta})$ and $\bar{C}_{irs}(\omega;\boldsymbol{\theta})$ are approximated in terms of $\boldsymbol{\theta}$ using quadratic polynomials; and every component of $\boldsymbol{\theta}$ is uniformly distributed over the range $[-1,1]$. As a result, the modal velocities $\bar{v}_s(\omega;\boldsymbol{\theta})$ can be approximated by Legendre polynomials as

$$\bar{v}_s(\omega;\boldsymbol{\theta}) = \sum_{0\le|\mathbf{l}|\le n^p} \bar{w}_{sl_1l_2\cdots l_{n^\theta}}(\omega)\prod_{a=1}^{n^\theta} P_{l_a}(\theta_a) \quad \text{for } a = 1,2,...,n^{ROM} \tag{53}$$

Analytical solutions of Eq. (52) can be obtained by applying Eqs. (23) and (25). In the end, the ensemble-averaged power flow can be expressed in terms of $\bar{\mathbf{w}}_s(\omega)$ as

$$\begin{aligned} &E_{\boldsymbol{\theta}}\left[\Pi_i(\omega;\boldsymbol{\theta})\right] \\ &= \frac{1}{2}\sum_{s=1}^{n^{ROM}} \mathrm{Re}\left[\hat{\mathbf{f}}_{is}(\omega)^*\,\bar{\mathbf{w}}_s(\omega)\right] \\ &\quad -\frac{1}{2}\sum_{r=1}^{n^{ROM}}\sum_{s=1}^{n^{ROM}} \bar{\mathbf{w}}_r(\omega)^*\,\hat{\mathbf{C}}_{irs}(\omega)\,\bar{\mathbf{w}}_s(\omega) \end{aligned} \tag{54}$$

where $\hat{\mathbf{f}}_{is}(\omega)$ is the expanded force vector and $\hat{\mathbf{C}}_{irs}(\omega)$ is the expanded damping matrix.

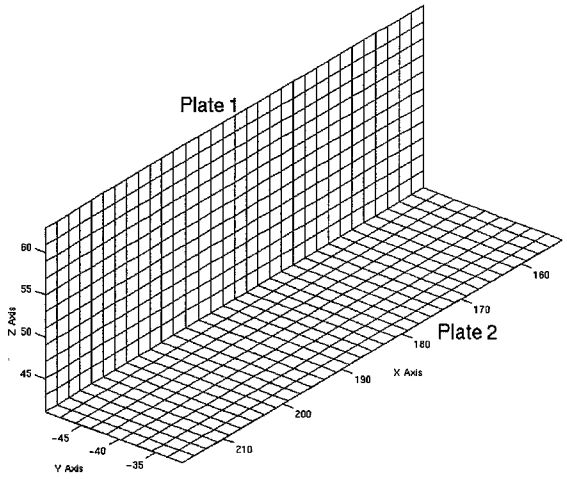

Fig. 4 The finite element mesh of the L-shaped plate. The dimensions and material properties are: Young's modulus $E = 2.9\times10^7$ psi, Poisson's ratio $\nu = 0.3$, density $\rho = 7.324\times10^{-4}$ lb/in^3, thickness $t = 0.4$ in.

The second application considers the variations of physical parameters of the system and their effects on the ensemble-averaged response of power flow. The example structure is the L-shaped plate that consists of two rectangular plates as shown in Fig. 4. Each plate is considered as a substructure. A variety of uncertainties may be associated with this structure, such as uncertainties in the connection angle or the thicknesses of the plates. A finite element model of this plate was constructed using NASTRAN quadrilateral plate elements (element CQUAD4, 4 nodes/element, 6 DOF/node). The finite element mesh yields 4158 DOF and an upper frequency limit of approximately 1000 Hz.

The thickness of Plate 1 is considered to be uncertain in this case study. The variation from the nominal value of the thickness is assumed to be associated with a uniformly distributed random parameter. Three finite element models are used such that the thickness of Plate 1 varies from -10% to +10% of the nominal thickness. After the global modal impedances and forces are computed for each FEM, quadratic polynomial approximations in terms of the random parameter θ, such as Eq. (29), are obtained by a least-square fit. For modal quantities in high modal density regions, this approximation is coarse so that a cubic spline approximation may be more suitable. However, for very large systems, this process, which includes rebuilding the FEM, could require considerable computational effort.

Plate 2 is excited along the free edge lengthwise. The ex-

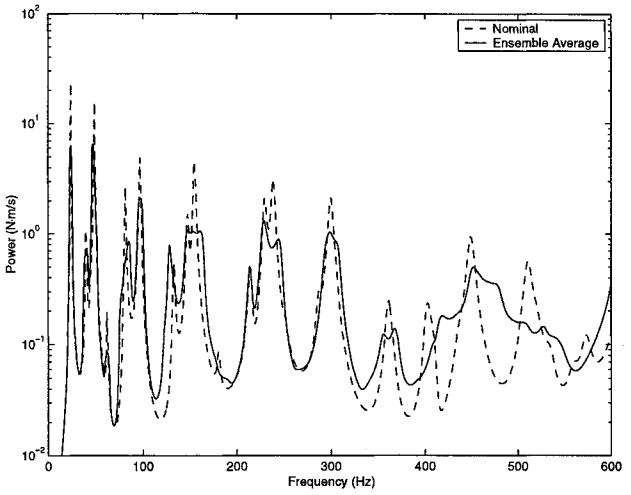

Fig. 5 Nominal and ensemble-averaged power flow from Plate 2 to Plate 1 of the L-shaped plate system.

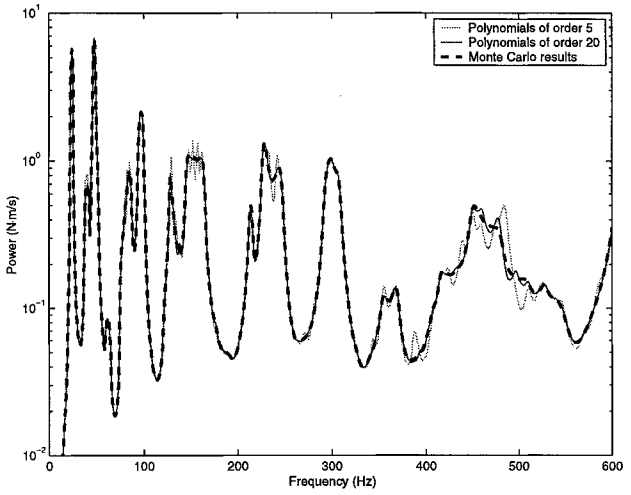

Fig. 6 Comparisons of the ensemble-averaged power flow calculated by Monte Carlo simulations and the approximations using Legendre polynomials of order 5 and order 20. The thickness of Plate 1 is varied from -10% to 10% of its nominal value.

ternal excitation is considered to be distributed sinusoidal point forces, of which the phases are assigned randomly so as to excite a large number of modes. The nominal value of power flow from Plate 2 to Plate 1 is first calculated and shown in Fig. 5. The ensemble-averaged power flow is also shown in Fig. 5 with 2000 realizations. This result has converged such that it is used as a benchmark for comparing other approximations. As can be seen in Fig. 5, the mean response is vastly different from the nominal response for frequencies above about 350 Hz. The implication is that the modes in this frequency range are more sensitive to uncertainties and polynomials of higher order are needed to capture the dramatic change.

Now the global modal velocities are approximated by Legendre polynomials of order 5 and 20, and then the ensemble-averaged power flow is calculated by Eq. (54). These results are compared in Fig. 6 to the Monte Carlo results. It is seen from Fig. 6 that the polynomial approximations have slower convergence around some resonant frequencies and at frequencies above 400 Hz. The same phenomenon was also seen in Fig. 3 in the previous section. Even though the approximation with polynomials of order 20 is needed to closely match the Monte Carlo results, the approximation with polynomials of order 5 provides a very good estimate of the ensemble-averaged power flow throughout the frequency range shown. Yet this low-order approximation yields at least two orders of magnitude fewer arithmetic operations relative to the Monte Carlo simulations. When the order of approximation is increased to 20, the computation time is still one order of magnitude less than that of Monte Carlo simulations.

Galerkin's Method with Locally Linear Interpolation Functions

The nominal power flow can be formulated using the CC modes or the global modes of the ROM. As mentioned in the previous section, the formulation using the global modes of the ROM is more suitable for deriving statistical approximations since the resultant approximations will be more computationally efficient. Therefore, the nominal power flow obtained from Eq. (18) and its corresponding system equations of motion, Eq. (16), are considered here. The modal velocities are approximated by a set of piecewise (locally-based) functions in place of the globally orthogonal polynomials. This results in a finite-element-like discretization over the random parameter space. This method will not necessarily yield faster convergence of the solution, but it permits the use of low-degree polynomials as the basis functions and thus allows a simpler and more general implementation.

Let Ω be the domain of $\boldsymbol{\theta}$. It is assumed that each component of $\boldsymbol{\theta}$ is only probable within the range $[-1, 1]$ such that Ω is a hypercube. Any bounded pdf can be assigned to this random variable set $\boldsymbol{\theta}$. Furthermore, Ω is assumed to consist of subdomains Ω^e such that $\Omega = \bigcup_{e=1}^{n^E} \Omega^e$, where n^E indicates the number of elements (subdomains) that constitutes the entire parameter space. It is assumed that $\bar{v}_b$, a component of the velocity vector $\bar{\mathbf{v}}$, may be approximated as

$$\bar{v}_b(\omega;\boldsymbol{\theta}) = \mathbf{N}(\boldsymbol{\theta})\,\mathbf{a}_b(\omega) = \sum_{e=1}^{n^E} \mathbf{N}^e(\boldsymbol{\xi})\,\mathbf{a}_b^e(\omega) \qquad (55)$$

where $\mathbf{N}(\boldsymbol{\theta})$ is the global (the entire random parameter space) shape function while $\mathbf{N}^e(\boldsymbol{\xi})$ is the local shape function, with $\boldsymbol{\xi}$ representing the local coordinates; $\mathbf{a}_b$ and $\mathbf{a}_b^e$ are the corresponding global and local nodal coordinates, which are the unknowns to be solved for. Considering a simple case with three random variables such that

$$\boldsymbol{\theta} = \begin{bmatrix} \theta_1 & \theta_2 & \theta_3 \end{bmatrix}^T, \quad \boldsymbol{\xi} = \begin{bmatrix} \xi_1 & \xi_2 & \xi_3 \end{bmatrix}^T \qquad (56)$$

The random parameter space could be meshed by 8-node "brick" elements and $\mathbf{N}^e(\boldsymbol{\xi})$ could be represented by

$$\mathbf{N}^e(\boldsymbol{\xi}) = \begin{bmatrix} N_1^e & N_2^e & \cdots & N_8^e \end{bmatrix} \qquad (57)$$

which is a vector of linear interpolation functions such that

$$N_i^e = \frac{1}{8}\left(1+s_{i1}\xi_1\right)\left(1+s_{i2}\xi_2\right)\left(1+s_{i3}\xi_3\right) \tag{58}$$

where s_{ij} is a component of the matrix $\mathbf{s}$ such that

$$\mathbf{s} = \begin{bmatrix} -1 & 1 & -1 & 1 & -1 & 1 & -1 & 1 \\ -1 & -1 & 1 & 1 & -1 & -1 & 1 & 1 \\ -1 & -1 & -1 & -1 & 1 & 1 & 1 & 1 \end{bmatrix}^T \tag{59}$$

For cases with more than three random variables, hypercube elements may be used and the vector of linear interpolation functions can be readily extended to higher dimensions. First, Galerkin's method is applied to Eq. (48) with the provided shape function $\mathbf{N}(\boldsymbol{\theta})$, yielding:

$$\begin{aligned} &\int_\Omega p(\boldsymbol{\theta})\,\mathbf{N}(\boldsymbol{\theta})^T \bar{z}_b(\omega;\boldsymbol{\theta})\,\mathbf{N}(\boldsymbol{\theta})\,\mathbf{a}_b(\omega)\,d\Omega \\ &= \int_\Omega p(\boldsymbol{\theta})\,\mathbf{N}(\boldsymbol{\theta})^T f_b(\omega;\boldsymbol{\theta})\,d\Omega \\ &\quad \text{for } b = 1,\ldots n^{ROM} \end{aligned} \tag{60}$$

Next, noting that $\mathbf{a}_b(\omega)$ is a constant with respect to the integration, it is taken out of the integral on the left-hand side of Eq. (60). This integral is then expressed as the sum of integrals over the subdomains

$$\begin{aligned} &\int_\Omega p(\boldsymbol{\theta})\,\mathbf{N}(\boldsymbol{\theta})^T \bar{z}_b(\omega;\boldsymbol{\theta})\,\mathbf{N}(\boldsymbol{\theta})\,d\Omega \\ &= \sum_{e=1}^{n^E}\int_{\Omega^e} p(\boldsymbol{\xi})\,\bar{z}_b^e(\omega;\boldsymbol{\xi})\,\mathbf{N}^e(\boldsymbol{\xi})^T\mathbf{N}^e(\boldsymbol{\xi})\left|\frac{\partial\Omega}{\partial\Omega^e}\right| d\Omega^e \\ &= \sum_{e=1}^{n^E}\int_{\Omega^e} p(\boldsymbol{\xi})\,\bar{z}_b^e(\omega;\boldsymbol{\xi}) \\ &\quad \begin{bmatrix} N_1^eN_1^e & N_1^eN_2^e & \cdots & N_1^eN_8^e \\ & N_2^eN_2^e & \cdots & N_2^eN_8^e \\ & & \ddots & \vdots \\ \text{symm} & & & N_8^eN_8^e \end{bmatrix} \left|\frac{\partial\Omega}{\partial\Omega^e}\right| d\Omega^e \end{aligned} \tag{61}$$

Thus, the modal impedance, $\bar{z}_b$, is discretized by Eq. (61), and the integrations of each element impedance in Eq. (61) are performed numerically by applying efficient Gaussian Quadrature schemes. Similarly, the right-hand side of Eq. (60) is given by

$$\begin{aligned} &\int_\Omega p(\boldsymbol{\theta})\,\mathbf{N}(\boldsymbol{\theta})^T f_b(\omega;\boldsymbol{\theta})\,d\Omega \\ &= \sum_{e=1}^{n^E}\int_{\Omega^e} p(\boldsymbol{\xi}) \begin{bmatrix} N_1^e \\ N_2^e \\ \vdots \\ N_8^e \end{bmatrix} \bar{f}_b^e(\omega;\boldsymbol{\xi})\left|\frac{\partial\Omega}{\partial\Omega^e}\right| d\Omega^e \end{aligned} \tag{62}$$

Hence, Eq. (60) can be cast into the matrix form

$$\hat{\mathbf{z}}_b\mathbf{a}_b = \hat{\mathbf{f}}_b \qquad \text{for } b = 1,2,\ldots,n^{ROM} \tag{63}$$

where $\hat{\mathbf{z}}_b$ is the impedance matrix for which the elements are obtained from Eq. (61), and $\hat{\mathbf{f}}$ is the force vector for which the elements are given from Eq. (62). From Eq. (51), the ensemble-averaged power flow is now expressed by

$$\begin{aligned} &E_{\boldsymbol{\theta}}\left[\Pi_i(\omega;\boldsymbol{\theta})\right] \\ &= \frac{1}{2}\sum_{b=1}^{n^{ROM}} \mathrm{Re}\left[\int_\Omega p(\boldsymbol{\theta})\,\bar{f}_{ib}(\omega;\boldsymbol{\theta})^*\,\bar{v}_b(\omega;\boldsymbol{\theta})d\Omega\right] \\ &\quad -\frac{1}{2}\sum_{b=1}^{n^{ROM}}\sum_{c=1}^{n^{ROM}}\int_\Omega p(\boldsymbol{\theta})\,\bar{v}_b(\omega;\boldsymbol{\theta})^* \\ &\quad \bar{C}_{bc}(\omega;\boldsymbol{\theta})\bar{v}_c(\omega;\boldsymbol{\theta})d\Omega \\ &= \frac{1}{2}\sum_{b=1}^{n^{ROM}} \mathrm{Re}\left[\left(\int_\Omega p(\boldsymbol{\theta})\,\mathbf{N}(\boldsymbol{\theta})^T\bar{f}_{ib}(\omega;\boldsymbol{\theta})d\Omega\right)^*\right. \\ &\quad \left.\mathbf{a}_b(\omega)\right] - \frac{1}{2}\sum_{b=1}^{n^{ROM}}\sum_{c=1}^{n^{ROM}}\mathbf{a}_b(\omega)^* \\ &\quad \left(\int_\Omega p(\boldsymbol{\theta})\,\mathbf{N}(\boldsymbol{\theta})^T\bar{C}_{ibc}(\omega;\boldsymbol{\theta})\mathbf{N}(\boldsymbol{\theta})d\Omega\right)\mathbf{a}_c(\omega) \\ &= \frac{1}{2}\sum_{b=1}^{n^{ROM}} \mathrm{Re}\left[\hat{\mathbf{f}}_{ib}(\omega)^*\,\mathbf{a}_b(\omega)\right] \\ &\quad -\frac{1}{2}\sum_{b=1}^{n^{ROM}}\sum_{c=1}^{n^{ROM}}\mathbf{a}_b(\omega)^*\,\hat{\mathbf{C}}_{ibc}(\omega)\,\mathbf{a}_c(\omega) \end{aligned} \tag{64}$$

where $\hat{\mathbf{f}}_{ib}(\omega)$ and $\hat{\mathbf{C}}_{ibc}(\omega)$ are defined by

$$\hat{\mathbf{f}}_{ib}(\omega) = \int_\Omega p(\boldsymbol{\theta})\,\mathbf{N}(\boldsymbol{\theta})^T\bar{f}_{ib}(\omega;\boldsymbol{\theta})d\Omega \tag{65}$$

$$\hat{\mathbf{C}}_{ibc}(\omega) = \int_\Omega p(\boldsymbol{\theta})\,\mathbf{N}(\boldsymbol{\theta})^T\bar{C}_{ibc}(\omega;\boldsymbol{\theta})\mathbf{N}(\boldsymbol{\theta})d\Omega \tag{66}$$

These integrals are evaluated by estimating the element-wise integrals numerically, like the formulations used in Eq. (61) and (62). With $\mathbf{a}_b(\omega)$ obtained as the solution to Eq. (63), the ensemble-averaged power flow can then be calculated from Eq. (64).

The L-shaped plate considered in the previous section is now used for numerical demonstration of this statistical approximation. The thicknesses of Plate 1 and Plate 2 as well as the connection angle between two plates are now considered to be uncertain. Thus, these three physical system parameters are associated with three independent, uniformly-distributed, random perturbations, such that Eq. (56) is assumed. In Eq. (56), θ_1 is associated with the variation of the thickness of Plate 1, θ_2 is associated with that of Plate 2, and θ_3 is associated with variation of the connection angle. It is assumed that the thicknesses of Plate 1 and Plate 2 vary from their nominal values by $\pm 10\%$, while the connection angle varies from its nominal value (90 degrees) by $\pm 20\%$.

In order to evaluate the ensemble-averaged power flow from Plate 2 to Plate 1 by using Eq. (64), the descriptions of $\bar{f}_{ib}(\omega;\boldsymbol{\theta})$ and $\bar{C}_{ibc}(\omega;\boldsymbol{\theta})$ in terms of $\boldsymbol{\theta}$ are supposed to

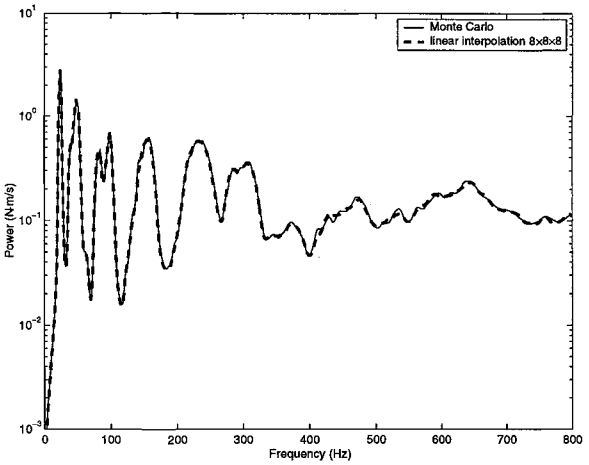

Fig. 7 Comparisons of the ensemble-averaged power flow calculated by Monte Carlo simulations and the approximation using locally linear interpolation functions with the random parameter space meshed by $8 \times 8 \times 8$ elements. The thicknesses of Plate 1 and Plate 2 are varied from -10% to 10% of their nominal values, while the connection angle is varied from -20% to 20% of its nominal value.

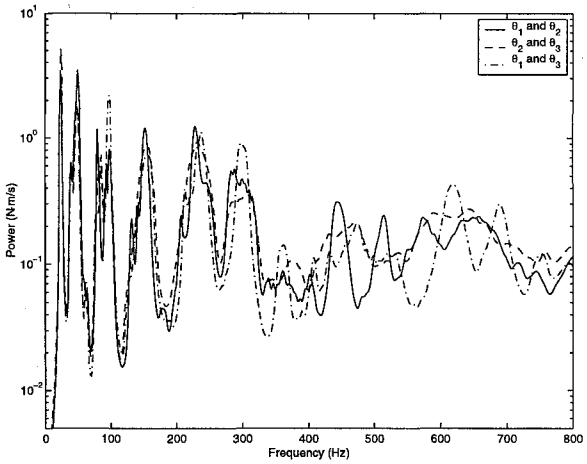

Fig. 8 Frequency response of the ensemble-average power flow for cases with two random parameters using the same system set-up as Fig. 7.

be known a priori, such that Eqs. (65) and (66) can be evaluated. As mentioned previously, the element-wise integrations of Eqs. (65) and (66) are performed by using Gaussian Quadrature methods, in which discrete data points of the integrands are needed. The discrete data points of $\bar{f}_{ib}(\omega;\boldsymbol{\theta})$ and $\bar{C}_{ibc}(\omega;\boldsymbol{\theta})$ are obtained by interpolating the data from 125 FEMs of this varying system. Moreover, in Eq. (64), the number of DOF of the ROM is fixed at 83, which provides accurate results up to 800 Hz for the power flow in the nominal system.

Figure 7 shows the results of the ensemble-averaged power flow considering the variations of the three physical parameters. The excitation is a sinusoidal force distributed along an edge of Plate 2 as in the previous case. When applying the approximation using locally linear interpolation (LLI) functions, or Eq. (64), the parameter domain is divided into $8 \times 8 \times 8$ cube elements. In Fig. 7, it is seen that the results from the LLI approximation closely match those from Monte Carlo simulations using 1,000 realizations. Since these results have clearly converged, the sensitivities of the system relative to the variations of the parameters can be further examined. Now based on this system set-up, θ_3 is fixed at zero such that the only random parameters are θ_1 and θ_2. The ensemble-averaged power flow of this case is shown in Fig. 8. Next, θ_1 and θ_2 are alternately fixed at zero, and the power flow results are also shown in Fig. 8. The distributions of total transmitted power in the frequency range of $[0, 800]$ Hz for these three cases are shown in Fig. 9. These sensitivity information can be readily retrieved from this approximation. Plate 1 and Plate 2 are nominally similar, so that power flow is strongest when the thicknesses are identical. These results agree with the findings of Ref. 11. Furthermore, this system is less sensitive to small variations in the connection angle when the nominal connection angle is 90 degrees, as shown in Ref. 12.

Conclusions

Considering the variations of system parameters, approximations for the ensemble-averaged power flow were presented. These statistical approximations are based on the nominal power flow formulations presented in Ref. 4, which employ characteristic constraint (CC) modes to capture the motion of the interface between component structures. In this paper, each modal response was expanded in a series of globally orthogonal polynomials or locally linear interpolation functions in terms of the random system parameters. Then, the system equations were derived using Galerkin's method such that the averaged power flow could be solved for.

The approximation using globally orthogonal polynomials was presented first. The choice of classical sets of orthogonal polynomials is based upon the pdf associated with the set of uncorrelated random system parameters. This approximation is versatile enough to accommodate the variations of both modal parameters and physical system parameters. The first application considered the random parameters to be associated with the component modal stiffnesses. The approximation with polynomials of order 3 compared very well to the Monte Carlo results for small variations of the parameters. Yet an approximation with polynomials of order 5 was needed to give satisfactory results when the variations were large. The next application considered the variation of the thickness of a L-shaped plate system. The approximations of the global modal quantities in terms of the random parameters were first obtained. Then two approximations with polynomials of low and high orders were shown to match the Monte Carlo results with different degree of convergence.

Next, the approximation using locally linear interpolation (LLI) functions was presented. This approximation enables a simpler and more systematic implementation that can be applied to a variety of systems. The system of the L-shaped plate with three uncertain physical parameters was

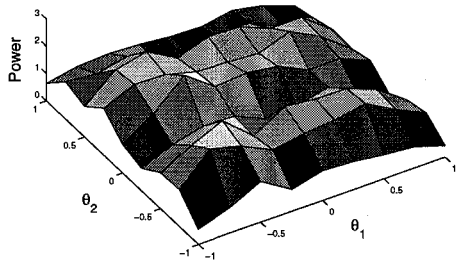

(a)

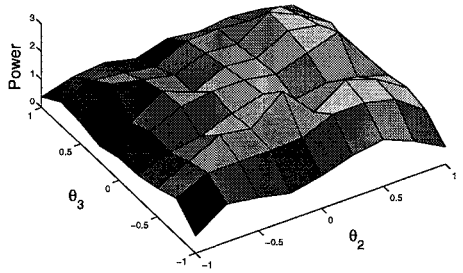

(b)

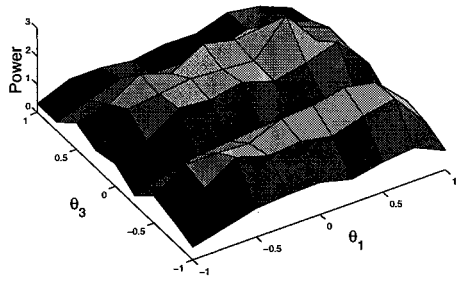

(c)

Fig. 9 The distributions of total transmitted power with respect to two system parameters correspond to the three cases shown in Fig. 8. (a) The power flow with respect to θ_1 and θ_2. (b) The power flow with respect to θ_2 and θ_3. (c) The power flow with respect to θ_1 and θ_3.

considered. The LLI results were seen to closely match the Monte Carlo results. Furthermore, sensitivity analyses can be readily performed by using this approximation.

In general, these statistical approximations are much more computationally efficient than Monte Carlo methods when obtaining the same degree of accuracy. In addition to fast convergence of the mean power flow, these approximations, unlike Monte Carlo simulation, provide insight into the behavior and sensitivity of the system under different parameter uncertainties, since the full description of every modal velocity in terms of the random parameters is also obtained using this approach.

References

[1]Lyon, R. H., *Statistical Energy Analysis of Vibrating Systems*, MIT Press, Cambridge, MA, 1975.

[2]Lyon, R. H. and DeJong, R. G., *Theory and Application of Statistical Energy Analysis*, Butterworth–Heinemann, Boston, 2nd ed., 1995.

[3]Lyon, R. H., "SEA, Power Flow, and Energy Accountancy," *SAE Paper 951303*, 1995.

[4]Tan, Y. C., Castanier, M. P., and Pierre, C., "Characteristic-Mode-Based Component Mode Synthesis For Power Flow Analysis in Complex Structures," *Proceedings of the 41st AIAA/ASME/ASCE/AHS/ASC Structures, Structural Dynamics, and Materials Conference and Exhibit*, Atlanta, GA, April 2000.

[5]Craig, R. R., "Substructure Methods in Vibration," *ASME Journal of Mechanical Design*, Vol. 117B, 1995, pp. 207–213.

[6]Seshu, P., "Substructuring and Component Mode Synthesis," *Shock and Vibration*, Vol. 4, No. 3, 1997, pp. 199–210.

[7]Castanier, M. P., Tan, Y. C., and Pierre, C., "Characteristic Constraint Modes For Component Mode Synthesis," *Proceedings of The 1999 ASME Design Engineering Technical Conference*, Las Vegas, NV, 1999.

[8]Papadimitrou, C., Katafygiotis, L. S., and Beck, J. L., "Approximate Analysis of Response Variability of Uncertain Linear System," *Probabilistic Engineering Mechanics*, Vol. 10, 1995, pp. 251–264.

[9]Iwan, W. D. and Jensen, H., "On the Dynamic Response of Continuous Systems Including Model Uncertainty," *ASME Journal of Applied Mechanics*, Vol. 60, 1993, pp. 484–490.

[10]Craig, R. R. and Bampton, M. C. C., "Coupling of Substructures for Dynamics Analyses," *AIAA Journal*, Vol. 6, No. 7, 1968, pp. 1313–1319.

[11]Boisson, C., Guyader, J. L., Millot, P., and Lesueur, C., "Energy Transmission in Finite Coupling Plates Part II: Application to an L Shaped Structure," *Journal of Sound and Vibration*, Vol. 81, No. 1, 1982, pp. 93–105.

[12]Rebillard, E. and Guyader, J. L., "Vibrational Behavior of a Population of Coupled Plates: Hypersensitivity to the Connexion Angle," *Journal of Sound and Vibration*, Vol. 188, No. 3, 1995, pp. 435–454.